Original article

Analytical relationships for mechanical properties of pentamode metamaterials

Reza Hedayati[a,*] , Kaivan Mohammadi[b], Sattar Jedari Salami[c], Nima Roudbarian[d], Pooyan Nayyeri[e], Mohamad Mahdi Rafiee[d], Habiba Bougherara[e]

[a]Faculty of Aerospace Engineering, Delft University of Technology (TU Delft), Kluyverweg 1, 2629 HS, Delft, The Netherlands

[b]Advanced Manufacturing Laboratory, School of Mechanical Engineering, Sharif University of Technology, Azadi Ave., Tehran, Iran

[c]Department of Biomedical Engineering, Central Tehran branch, Islamic Azad University, Tehran, Iran

[d]School of Mechanical Engineering, College of Engineering, University of Tehran, Tehran, Iran

[e]Department of Mechanical and Industrial Engineering, Toronto Metropolitan University, Toronto, ON, Canada

*Corresponding author. Email: r.hedayati@tudelft.nl, rezahedayati@gmail.com.

Abstract

Pentamode metamaterials are a class of extremal materials exhibiting fluid-like mechanical behavior. The mechanical properties of pentamode metamaterials arise from their unique micro-architecture, rather than their constituent material. In this research, we present closed-form analytical relationships for the elastic modulus and Poisson's ratio of pentamode lattice structures with double-cone struts based on cubic diamond morphology. To validate our analytical solutions, we performed numerical simulations and experimental tests, which confirmed the accuracy of the derived relationships. Our findings indicate that increasing the smaller diameter (d) and the larger-to-smaller diameter ratio (α) of the double-cones increases the elastic modulus of pentamode metamaterials. However, within the considered range of d and α, the Poisson's ratio is nearly constant and lies within the range of approximately 0.5. These analytical relationships provide valuable insight into the mechanical behavior of pentamode metamaterials, which can aid in the design and optimization of new materials with unique properties.

Keywords: *Pentamodes; Lattice Structure; 3D Printing; Analytical Solution*

1. Introduction

Recent advances in the development of lattice structures, known as metamaterials, has expanded the range of realizable mechanical properties [1-3]. Auxetics [4, 5], Pentamodes [6-8], acoustic metamaterials [9, 10], smart active lattices [11, 12], and structures with negative compressibility [13, 14] are the most common metamaterials. Pentamode metamaterials are rationally designed man-made structures which offer shear moduli orders of magnitude smaller than their bulk moduli [15-17]. That is why some pentamodes are also sometimes referred to meta-fluids as they can deform in shear much easier than under normal forces [18].

Pentamode metamaterials were first suggested theoretically in 1995 by Milton and Cherkaev [19]. They proposed a cubic diamond lattice with double-cone struts as a good example of metamaterials, and since, the majority of the works in the field of metamaterials has been dedicated to the noted micro-architecture. However, despite the fact that the pentamode can offer exceptional interesting properties, they were not realized experimentally until very recently in 2012 [18] due to complexities present in their manufacturing. Additive manufacturing, also known as 3D printing technologies, have made manufacturing of pentamode significantly more convenient, and this has led to an exponential growth in works dedicated to pentamodes [20-27].

The increased application of pentamodes as building blocks in the making of novel structures highlights the importance of deriving analytical relationships for these structures. Using analytical formulas facilitates the application of pentamodes in the design process of novel engineering designs [28, 29]. A main barrier in deriving analytical relationships for pentamodes is the fact they are composed of struts with variable cross-sections. In a recent work [30], we presented semi-analytical relationships for elastic modulus, Poisson's ratio, and yield strength of pentamodes. The semi-analytical relationships were solved using the Ritz method and gave acceptable results. Our analytical work presented in [30] had the drawback of being of open-form, requiring extensive computational techniques which intrinsically adds some unwanted approximations to the acquired results. Closed-form solutions, on the other hand, do not require expensive computational solutions and can be solved instantaneously. Additionally, due to their nature of giving the final answer explicitly in terms of the model variable, they give the exact solution within the assumptions considered during the derivations.

In this work, for the first time, we present analytical relationships for the elastic modulus and Poisson's ratio of pentamode structures. As for the first step, closed-form formulas are obtained for double-cone beams using the Timoshenko beam theory. The obtained relationships are then implemented in deriving the analytical solutions for the pentamode lattice structure. Numerical methods are used in both steps for verifications. Moreover, several pentamode lattice structures are manufactured and tested mechanically to evaluate the accuracy of the analytical solutions.

2. Materials and methods

2.1. Analytical solution for double-cone beams

Here, we want to obtain closed-form analytical relationships for a cantilever beam with variable circular cross-section. The governing equations of Timoshenko beam theory are:

$$-\frac{d}{dx}\left(E_s I \frac{d\phi}{dx}\right) + \kappa A_s G_s \left(\phi + \frac{dw}{dx}\right) = 0 \tag{1}$$

$$-\frac{d}{dx}\left(\kappa A G_s \left(\phi + \frac{dw}{dx}\right)\right) = q \tag{2}$$

where E_s and G_s are respectively the elastic modulus and shear modulus of the matrix material, I and A are respectively the area moment of inertia and cross-sectional area, w and ϕ are respectively the beam deflection and the angle of rotation of the normal to the mid-surface of the beam, κ is the shear coefficient factor, q is the function of distributed load, and x is direction parallel to beam main axis. Combining Eqs. (1) and (2) gives:

$$\frac{d^2}{dx^2}\left(E_s I \frac{d\phi}{dx}\right) = q \tag{3}$$

Since the distributed load is zero, Eq. (3) simplifies to:

$$\frac{d^2}{dx^2}\left(E_s I \frac{d\phi}{dx}\right) = 0 \tag{4}$$

Integrating from Eq. (4) gives:

$$Q_{xx} = \frac{d}{dx}\left(E_s I \frac{d\phi}{dx}\right) = C_1 \tag{5}$$

$$M_{xx} = E_s I \frac{d\phi}{dx} = C_1 x + C_2 \tag{6}$$

The parameters I and A depend on x since the cross-section is not constant along the x direction (Figure 1). The radius changes along the x axis according to:

$$r(x) = \begin{cases} r_1(x) = 2(R-r)\dfrac{x}{l} + r & 0 \le x \le l/2 \\ r_2(x) = -2(R-r)\dfrac{x-\dfrac{l}{2}}{l} + R & l/2 \le x \le l \end{cases} \tag{*}$$

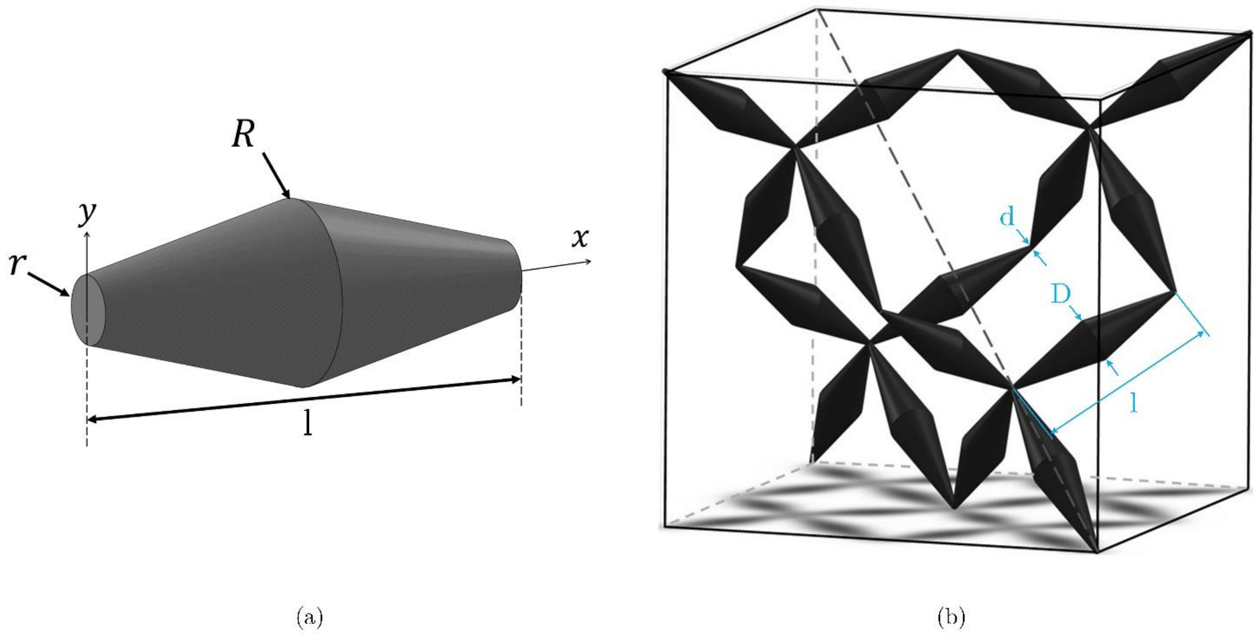

Figure 1: (a) Dimensions of a double-cone strut. (b) A pentamode unit cell structure

Similarly, $I_1(x)$ and $I_2(x)$ are the area moments of inertia for parts with radii of respectively $r_1(x)$ and $r_2(x)$. For $0 \le x \le l/2$, integrating from Eq. (6) gives:

$$\phi_1(x) = \int \frac{C_1 x + C_2}{E_s I_1(x)} dx + C_3 \tag{7}$$

By inserting Eq. (7) into Eq. (1), $w_1(x)$ can be found:

$$\begin{aligned} &\phi_1(x) + \frac{dw_1(x)}{dx} = \frac{1}{\kappa A_1(x)\, G_s} \frac{d}{dx}\left(E_s I_1(x) \frac{d\phi_1(x)}{dx}\right) \rightarrow \\ &w_1(x) = -\int \phi_1(x) dx + \frac{1}{\kappa A_1(x)\, G_s} E_s I_1(x) \frac{d\phi_1(x)}{dx} + C_4 \end{aligned} \tag{8}$$

By repeating the procedure for $l/2 \le x \le l$, we have:

$$\phi_2(x) = \int \frac{C_5 x + C_6}{E_s I_2(x)} dx + C_7 \tag{9}$$

$$w_2(x) = -\int \phi_2(x) dx + \frac{1}{\kappa A_2(x)\, G_s} E_s I_2(x) \frac{d\phi_2(x)}{dx} + C_8 \tag{10}$$

By performing the integration in Eqs. (7) and (9), we have:

$$\phi_1(x) = \frac{4l^4\left[-\frac{-lrC_1+2RC_2-2rC_2}{3(2R-2r)^2(2Rx+lr-2rx)^3}-\frac{C_1}{2(2R-2r)^2(2Rx+lr-2rx)^2}\right]}{\pi E_s}+C_3 \tag{11}$$

$$\phi_2(x) = \frac{4l^4\left[-\frac{2RlC_5-lrC_5+2RC_6-2rC_6}{(2R-2r)^2(-2Rl+2Rx+lr-2rx)^3}-\frac{C_5}{(2R-2r)^2(-2Rl+2Rx+lr-2rx)^2}\right]}{\pi E_s}+C_7 \tag{12}$$

By inserting $\phi_1(x)$ and $\phi_2(x)$ from Eqs. (11) and (12) into Eqs. (8) and (10), $w_1(x)$ and $w_2(x)$ can be found:

$$w_1(x) = -\frac{4l^4\left[-\frac{lrC_1+2RC_2-2rC_2}{6(2R-2r)^3\{(2R-2r)x+rl\}^2}+\frac{C_1}{2(2R-2r)^3\{(2R-2r)x+rl\}}\right]}{\pi E_s} - C_3x + \frac{xC_1+C_2}{\kappa\pi\left[\frac{2(R-r)x}{l}+r\right]^2 G_s}+C_4 \tag{13}$$

$$w_2(x) = -\frac{4l^4\left[\frac{C_5}{2(2R-2r)^3\{(2R-2r)x-2Rl+rl\}}+\frac{2RlC_5-lrC_5+(2R-2r)C_6}{6(2R-2r)^3\{(2R-2r)x-2Rl+rl\}^2}\right]}{\pi E_s} - C_7x + \frac{xC_5+C_6}{\kappa\pi\left[-\frac{2(R-r)(x-\frac{l}{2})}{l}+R\right]^2 G_s}+C_8 \tag{14}$$

There are four boundary conditions at the root and at the end of the beam. Moreover, four continuity conditions should be satisfied at the mid-span of the beam. We apply the boundary conditions to each of the cases interesting to this study: displacement without rotation and rotation without displacement.

a) Displacement without rotation at the end of the beam: The boundary conditions at $x=0$ are $w_1=0$ and $\phi_1=0$. The boundary conditions at $x=l$ are $w_2=\delta$ and $\phi_2=0$. Finally, the continuity conditions at the mid-spam are $w_1=w_2$, $\phi_1=\phi_2$, $M_{xx1}=M_{xx2}$, and $Q_{xx1}=Q_{xx2}$. The eight noted boundary conditions give eight equations with eight to-be-determined constants $C_i,\ i=1:8$. The set of equations can be written in a matrix form as follows:

$$[K_{ij}]_{8\times8}\{C_j\}_{8\times1}=[F_i]_{8\times1} \tag{15}$$

The coefficients C_i can be found by solving the set of equations in Eq. (14). By inserting C_5 and C_6 into:

$$\begin{cases} M_{xx} = E_s I_2(x) \dfrac{d\phi_2(x)}{dx} = C_5 x + C_6 \\ Q_{xx} = \dfrac{d}{dx}\left(E_s I_2(x) \dfrac{d\phi_2(x)}{dx}\right) = C_5 \end{cases} \tag{16}$$

the point load F_0 and concentrated moment M_0 at the end of the cantilever can be obtained. By setting $Q_{xx} = F_0 = C_5$ and $M_{xx} = M_0 = C_5 l + C_6$ at $x = l$, we have:

$$\begin{cases} F_0 = \left(\dfrac{3\pi\kappa G_s E_s R r^3}{\kappa G_s l^3 + 3E_s R r l}\right)\delta \\ M_0 = \dfrac{3\pi\kappa G_s E_s R r^3}{2(\kappa G_s l^2 + 3E_s R r)}\delta \end{cases} \tag{17}$$

b) Rotation without displacement at the end of the beam: The boundary conditions at $x = 0$ are $w_1 = 0$ and $\phi_1 = 0$. The boundary conditions at $x = l$ are $w_2 = 0$ and $\phi_2 = \theta$. Finally, the continuity conditions at the mid-span are $w_1 = w_2$, $\phi_1 = \phi_2$, $M_{xx1} = M_{xx2}$, and $Q_{xx1} = Q_{xx2}$.

By setting $Q_{xx} = F_0 = C_5$ and $M_{xx} = M_0 = C_5 l + C_6$ at $x = l$, we have:

$$\begin{cases} F_0 = \left\{\dfrac{\pi E_s R r^3 (7\kappa G_s R^2 l^2 - 7\kappa G_s R r l^2 - 3\kappa G_s r^2 l^2 + 12 E_s R^3 r - 12 E_s R^2 r^2)}{2l^2(R^2 - Rr - r^2)(\kappa G_s l^2 + 3E_s R r)}\right\}\theta \\ M_0 = \left\{\dfrac{\pi E_s R r^3 (6\kappa G_s R^2 l^2 - 7\kappa G_s R r l^2 - 3\kappa G_s r^2 l^2 + 9 E_s R^3 r - 12 E_s R^2 r^2)}{4l(R^2 - Rr - r^2)(\kappa G_s l^2 + 3E_s R r)}\right\}\theta \end{cases} \tag{18}$$

The parameters F_0 and M_0 are summarized in Table S1 in Supplementary Material accompanying the paper.

2.2. Analytical solution for penta-mode structure

Based on the procedure explained in the Supplementary Materials, the analytical relationship for the elastic modulus of pentamode metamaterial can be obtained as:

$$\left(\frac{E}{E_s}\right)_{EB} = \frac{3\sqrt{2}\pi R r}{4l^2 \cos\theta \left(\cos^2\theta \left(\frac{l}{r}\right)^2 + 3\sin^2\theta\right)} \tag{19}$$

If the shear deformation and rotational bending effects are taken into account (i.e., for calculations based on Timoshenko beam theory), the normalized elastic modulus is given by:

$$\left(\frac{E}{E_s}\right)_{T} = \frac{\pi\sqrt{2} R r}{4l^2 \cos\theta \left(\frac{\cos^2\theta}{3}\left(\frac{\kappa G_s l^2 + 3E_s R r}{\kappa G_s r^2}\right) + \sin^2\theta\right)} \tag{20}$$

As for the Poisson's ratio, the analytical relationship is obtained as:

$$\nu_{EB} = -\frac{\sqrt{2}}{2}\frac{r\sin\theta\cos\theta\left(\left(\frac{l}{r}\right)^2 - 3\right)}{\left(\cos^2\theta\left(\frac{l}{r}\right)^2 + 3\sin^2\theta\right)} \tag{21}$$

And the Poisson's ratio obtained based on Timoshenko beam theory is:

$$\nu_T = -\frac{\sqrt{2}}{2}\frac{\cos\theta\sin\theta\left(\frac{\kappa G_s l^2 + 3E_s Rr}{3\kappa r^2} - G_s\right)}{\frac{\cos^2\theta}{3}\left(\frac{\kappa G_s l^2 + 3E_s Rr}{\kappa r^2}\right) + G_s \sin^2\theta} \tag{22}$$

2.3. Numerical modeling

Finite element (FE) models were created using the COMSOL Multiphysics package (Stockholm, Sweden). As for the models dedicated to studying the mechanical response of double-cone beams exclusively, double-cone beams with a length of 3.4 mm were constructed and discretized using ~8000 volumetric 10-node tetrahedron element types. A linear elastic material model with elastic constants of titanium alloy Ti-6Al-4V ($E_s = 113$ GPa and $\nu = 0.33$) was assigned to the matrix material. Scripts were written to automatically vary the geometry of the beam structure and to record the results for different ratios of α. The root of the beam structure was constrained in all directions, while its other end was displaced laterally for 400 μm without permitting any rotation.

The pentamode lattice structures were created by stacking 5×5×5 unit cells in each direction each having a dimension of 8 mm (Figure 2). The lower face of the lattice structure was constrained in the Z direction, while they were free to move in the X and Y directions. One node in the lower face was constrained in all directions to avoid the rigid body motion of the whole structure. The nodes located at the upper face of the lattice structure were displaced downward for 1010 μm in a stepwise (in 10 steps) uniform fashion, and they were allowed to move in the X and Y directions freely. Based on the results of mesh sensitivity analysis, element sizes smaller than 20 μm and 140 μm at the smaller and larger diameters of each strut were used. Each lattice structure was discretized using ~10^6 elements. All the FE models were solved using MUMPS static solver in COMSOL.

2.4. Experimental tests

Structures with $\alpha = 1, 2, 3, 4$, and 5 were fabricated using Flashforge Foto 13.3 LCD 3D printer (Flashforge, China), see Figure 2. eSUN eResin-PLA Pro polymer (grey color) was used for manufacturing the body of the lattice structure, and the same resin was used to create a raft to hold the bottom of the lattice structure. Specimens were only manufactured for $d = 700\,\mu m$. The surface roughness of specimens was measured using a Sensofar S Neox 3D Optical Profiler (Sensofar, Spain). The surface roughness of the specimens was <1.486 μm confirming good production quality.

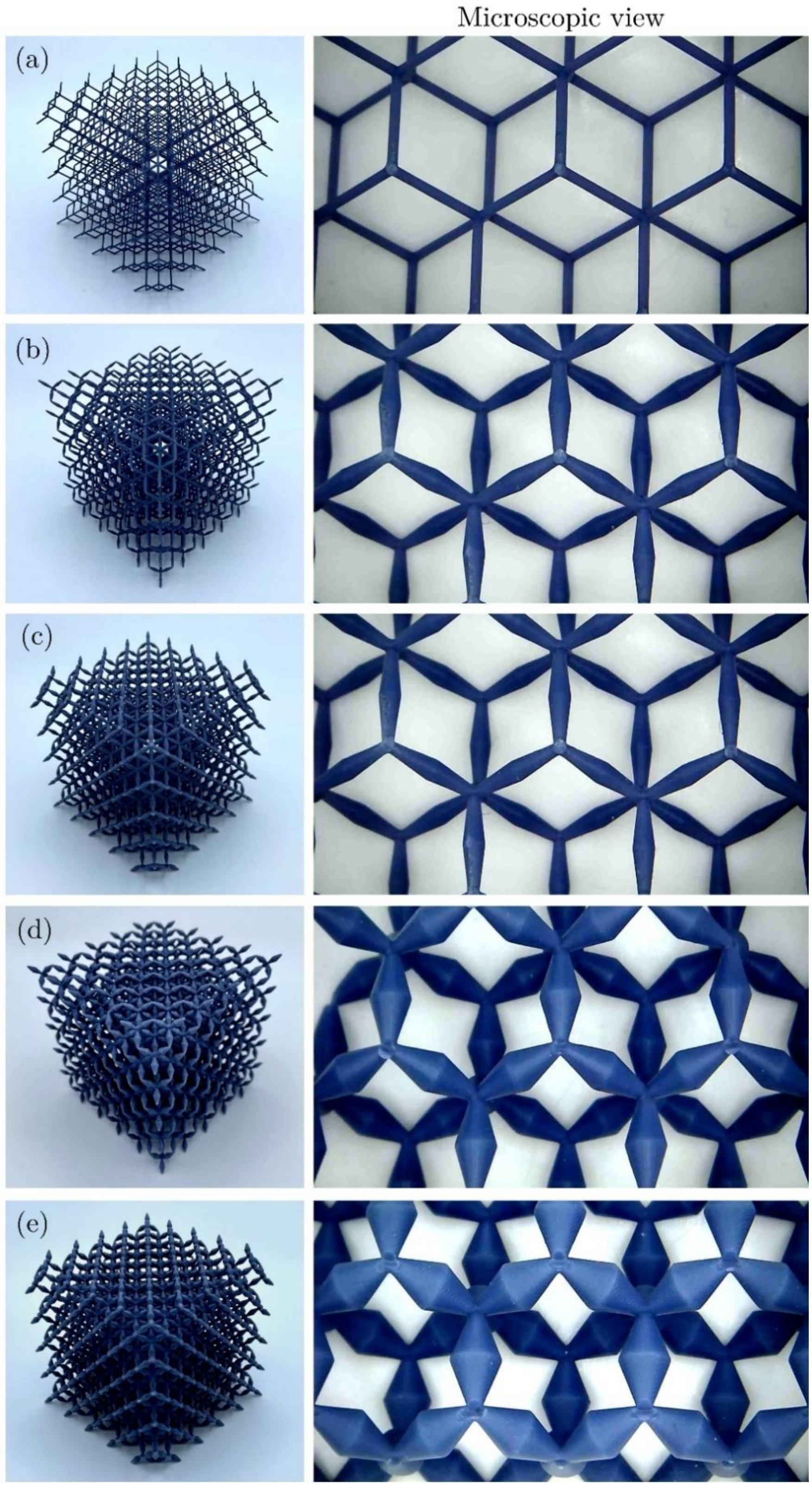

Figure 2: Manufactured specimens with (a) $\alpha = 1$, (b) $\alpha = 2$, (c) $\alpha = 3$, (d) $\alpha = 4$, (e) $\alpha = 5$.

A servo-hydraulic MTS 370 mechanical testing machine (Eden Prairie, MN, USA) with an MTS 661.20H-03 100 kN load cell was used to load the specimens under uniaxial compressive loads with a displacement rate of 5 mm/min. The linear elastic regime of the stress-strain curves was considered and implemented to obtain the elastic modulus and yield strength of the structures in accordance with ISO standard 13314:2011. The elastic modulus was normalized with respect to that of the constituent material ($E_s = 1.9$ GPa) for comparison purposes. To determine the Poisson's ratio of the specimens, image processing techniques were employed to capture and measure both lateral and axial displacements of the specimens during deformation.

3. Results

The results for force and moments of a cantilever beam for α up to 5 show exceptional agreement between numerical and analytical results for the case of the free end being displaced with no rotation (Figure S4 in the Supplementary Material accompanying the paper). Even for α as high as 10, the numerical/analytical discrepancy does not exceed 20%. The difference between numerical and analytical relationships for the case of a cantilever beam under axial loading is also exceptionally low for α up to 3 and is acceptable for α up to 5 (<15% difference). In summary, the three main cases of load-α curves examined, the analytical relationships of which formed the basis of the analytical relationships for pentamodes, were found to be sufficiently accurate and suitable for deriving the analytical relationships for mechanical properties of the lattice structure.

The numerical and analytical results are compared for different smaller diameter values from $d = 125\ \mu m$ to $d = 350\ \mu m$. The analytical results are plotted for two cases. In the first case, the vertex-to-vertex distance of the cubic diamond geometry which was the base for constructing the pentamode lattice was considered as strut length. In the second case, the overlapping effect was taken into account and the average struts length by neglecting the joint region was considered as the strut length. As it can be seen in Figure 3, there was very good agreement between numerical and analytical elastic modulus for all d values as well as for α up to ~ 5. The mean experimental elastic moduli at all α values were in good agreement with both numerical and analytical results and had <20% discrepancies (Figure 3c). In general, the experimental values were slightly smaller than the numerical/analytical values. This can be attributed to a decrease in the effective cross-sectional area in the struts of the fabricated specimens due to the inherent limitation of additive manufacturing in providing well-connected material adhesion in the bulk of the structure due to its layer-by-layer nature manufacturing process.

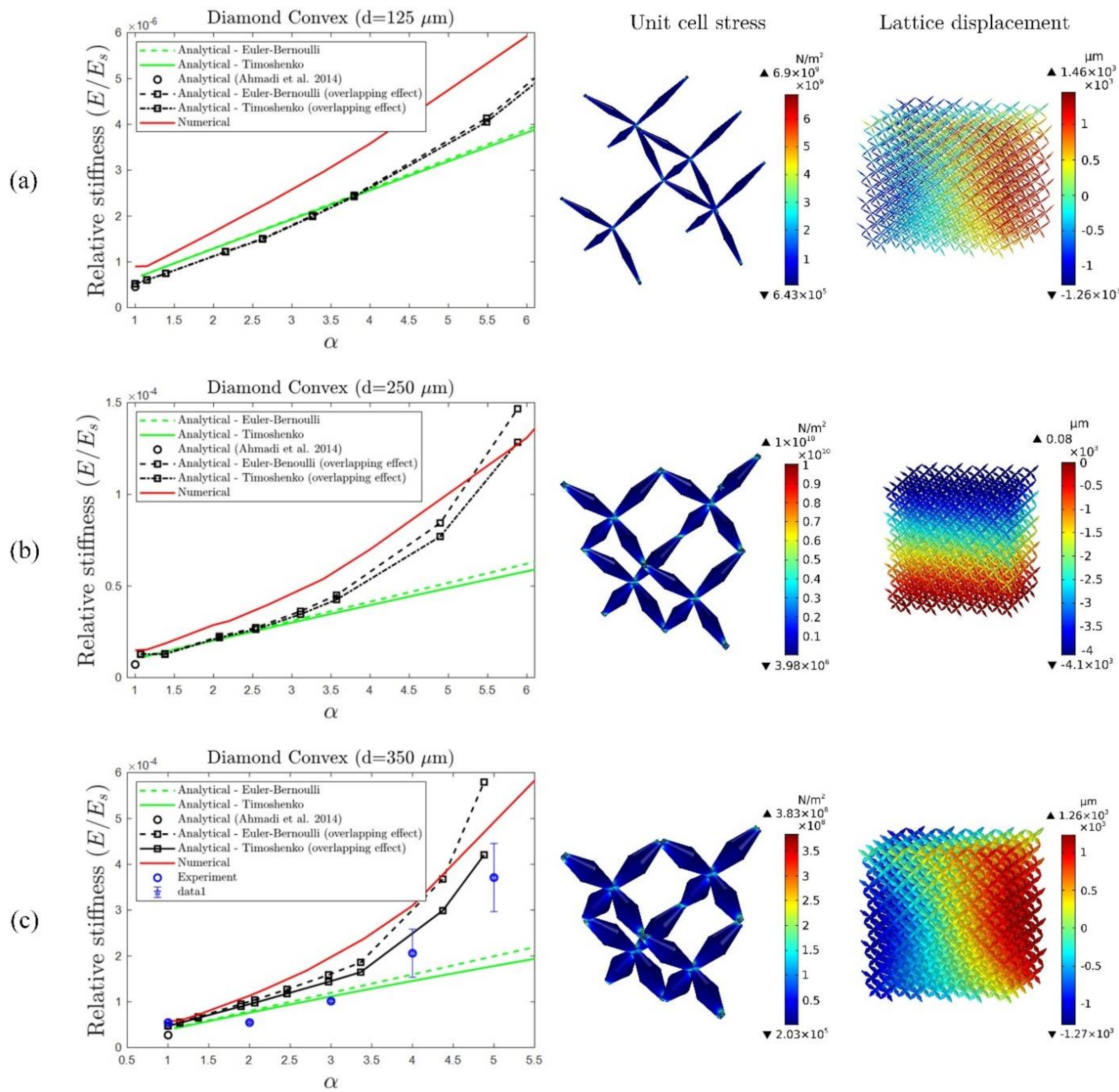

Figure 3: Comparison of analytical and numerical relative stiffness for pentamodes with (a) $d = 125\ \mu m$, (b) $d = 250\ \mu m$, and (c) $d = 350\ \mu m$.

The analytical relationships and numerical results predicted relatively constant Poisson's ratio ($\nu \approx 0.5$) values for all d and α values. The experimental values also confirmed the noted independency (Figure 4).

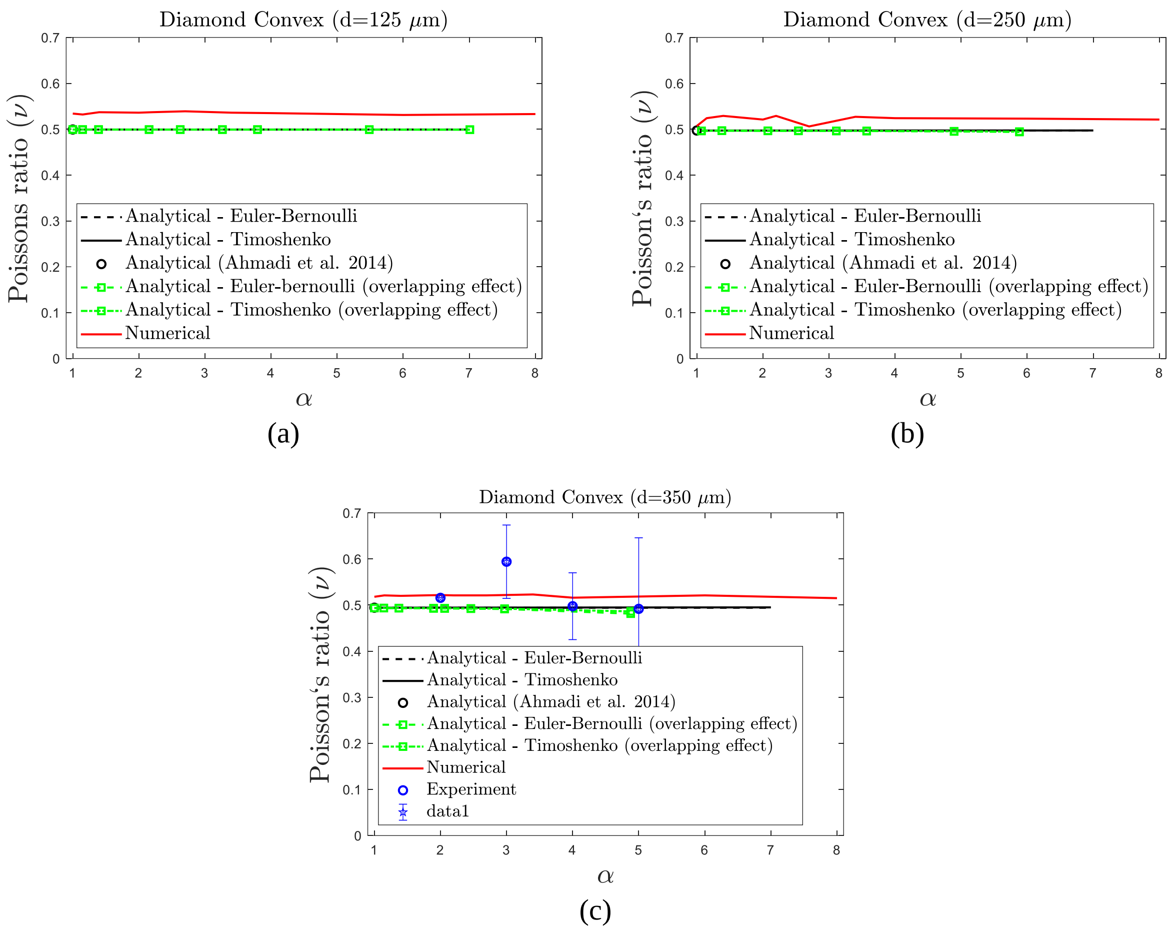

Figure 4: Comparison of analytical and numerical Poisson's ratio for pentamodes with (a) $\mathbf{d = 125\ \mu m}$, (b) $\mathbf{d = 250\ \mu m}$, and (c) $\mathbf{d = 350\ \mu m}$.

As the pentamodes are known for being able to demonstrate fluid-like behavior, the bulk modulus and shear modulus of these structures were measured numerically (Figure 5), and their B/G ratio (a.k.a. figures-of-merit or FOM) were calculated (Figure 6). It can be seen that as the d/l ratio decreases, the B/G ratio increases exponentially (Figure 6). For $d/l \approx 0.037$ (i.e., d=125 μm), FOM in the range of 200 was achieved. The FOM had a high dependency on the smaller diameter d, but a small dependency on the large diameter D. The results of this study can be used to design optimal lattice structures with non-uniform distribution of pentamode unit cells. A few examples of non-uniform or anisotropic designs without making use of analytical approaches in the design stage can be found in [2, 31-34].

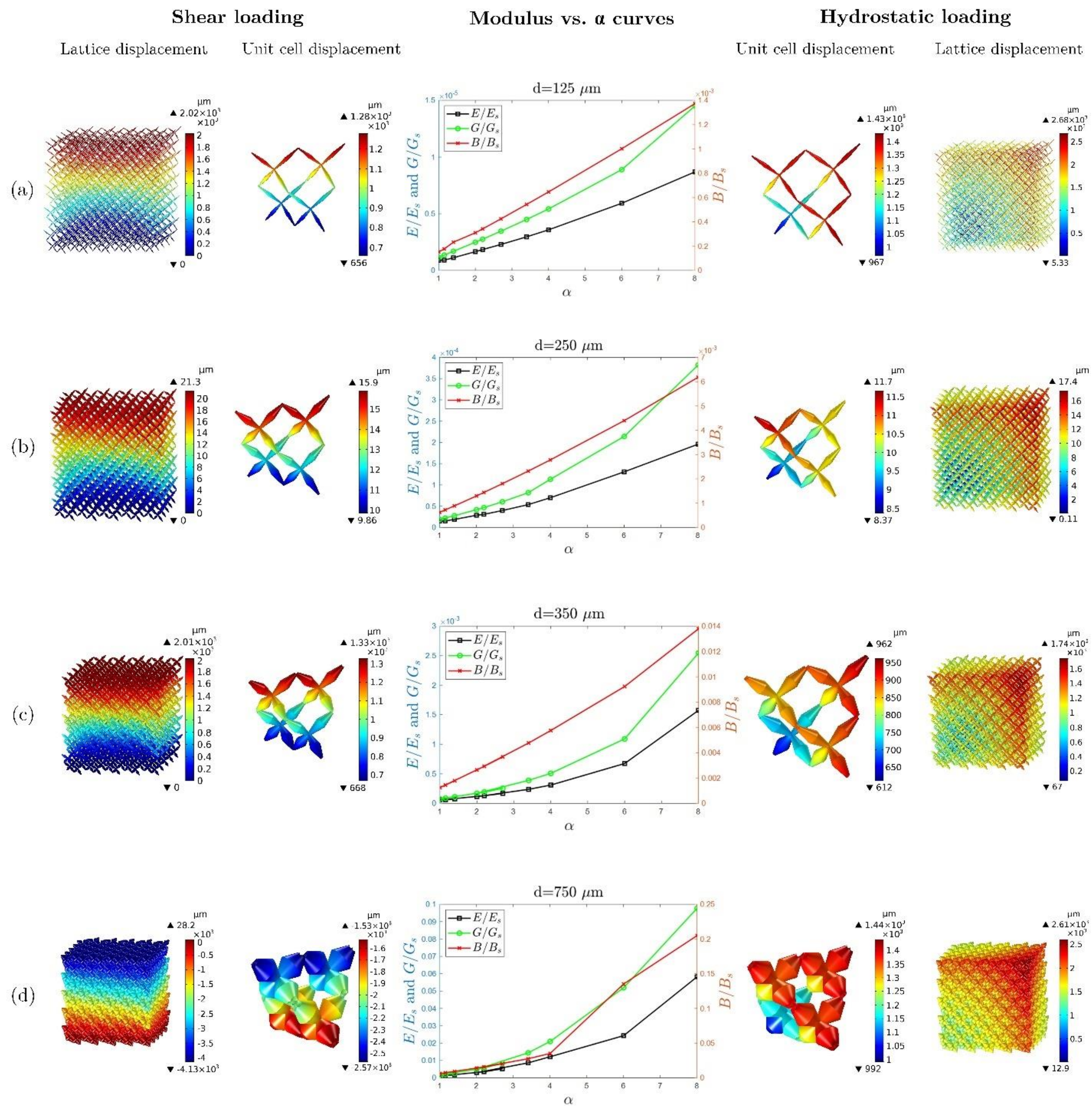

Figure 5: Variation of relative elastic modulus, shear modulus, and bulk modulus with respect to α for (a) $d = 125\ \mu m$, (b) $d = 250\ \mu m$, (c) $d = 350\ \mu m$, and (d) $d = 750\ \mu m$.

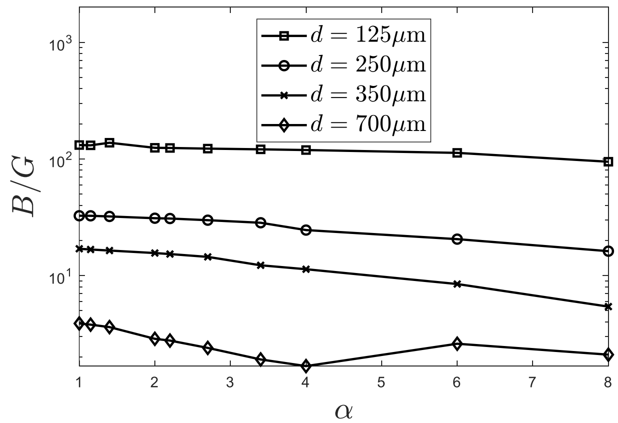

Figure 6: Variation of B/G with respect to α for different smaller diameter values.

5. Conclusions

This research has successfully derived closed-form analytical relationships for the elastic modulus and Poisson's ratio of double-cone beams and pentamode metamaterials based on diamond geometry. These analytical relationships have helped fill a significant gap in the field of pentamodes and offer a valuable tool for designing and analyzing these materials. The accuracy of these relationships was confirmed through comparisons with both numerical and experimental results. The results indicate that increasing the smaller diameter (d) and the larger to smaller diameter ratio (α) can increase the elastic modulus, while the Poisson's ratio remains almost independent of these variables and is consistently around 0.5 within the considered range. Additionally, the structures' figures-of-merit were highly influenced by the smaller diameter and minimally affected by the larger diameter of the double cones.

Acknowledgement

We would like to thank Mr. Babak Tarivirdilouy Asl for helping us in performing the numerical simulations.

References

1. Hai, L., Q. Zhao, and Y. Meng, *Unfeelable mechanical cloak based on proportional parameter transform in bimode structures.* Advanced Functional Materials, 2018. **28**(30): p. 1801473.
2. Mohammadi, K., M. Movahhedy, I. Shishkovsky, and R. Hedayati, *Hybrid anisotropic pentamode mechanical metamaterial produced by additive manufacturing technique* Applied Physics Letters, 2020. **117**(6): p. 061901.
3. Hedayati, R., A. Güven, and S. Van Der Zwaag, *3D gradient auxetic soft mechanical metamaterials fabricated by additive manufacturing.* Applied Physics Letters, 2021. **118**(14): p. 141904.
4. Han, D., X. Ren, Y. Zhang, X.Y. Zhang, X.G. Zhang, C. Luo, and Y.M. Xie, *Lightweight auxetic metamaterials: Design and characteristic study.* Composite Structures, 2022. **293**: p. 115706.
5. Zhang, X.Y., X. Ren, Y. Zhang, and Y.M. Xie, *A novel auxetic metamaterial with enhanced mechanical properties and tunable auxeticity.* Thin-Walled Structures, 2022. **174**: p. 109162.

6. Dong, H.-W., S.-D. Zhao, X.-B. Miao, et al., *Customized broadband pentamode metamaterials by topology optimization.* Journal of the Mechanics and Physics of Solids, 2021. **152**: p. 104407.
7. Guo, D., S. Jiang, Y. Zhou, L. Zhang, K. Li, B. Song, and Y. Huang, *Ultrahigh compression-shear ratio of sandwich pentamode metamaterials.* Composite Structures, 2023. **322**: p. 117331.
8. Huang, Y., X. Zhang, L. Zhang, and C. Cai, *Theoretical verification of three-dimensional manufacturable pentamode metamaterial microstructure.* Journal of Physics: Condensed Matter, 2021. **33**(48): p. 485702.
9. Hedayati, R. and S. Lakshmanan, *Pneumatically-Actuated Acoustic Metamaterials Based on Helmholtz Resonators.* Materials, 2020. **13**(6): p. 1456.
10. Muhammad and C. Lim, *From photonic crystals to seismic metamaterials: A review via phononic crystals and acoustic metamaterials.* Archives of Computational Methods in Engineering, 2022. **29**(2): p. 1137-1198.
11. Roudbarian, N., E. Jebellat, S. Famouri, M. Baniasadi, R. Hedayati, and M. Baghani, *Shape-memory polymer metamaterials based on triply periodic minimal surfaces.* European Journal of Mechanics-A/Solids, 2022: p. 104676.
12. Pishvar, M. and R.L. Harne, *Foundations for soft, smart matter by active mechanical metamaterials.* Advanced science, 2020. **7**(18): p. 2001384.
13. Ding, Y., Z. Liu, C. Qiu, and J. Shi, *Metamaterial with simultaneously negative bulk modulus and mass density.* Physical review letters, 2007. **99**(9): p. 093904.
14. Khan, K.A., M.H. Alshaer, and M.A. Khan, *A Novel Twofold Symmetry Architected Metamaterials with High Compressibility and Negative Poisson's Ratio.* Advanced Engineering Materials, 2021. **23**(5): p. 2001041.
15. Schittny, R., T. Bückmann, M. Kadic, and M. Wegener, *Elastic measurements on macroscopic three-dimensional pentamode metamaterials.* Applied Physics Letters, 2013. **103**(23): p. 231905.
16. Kadic, M., T. Bückmann, R. Schittny, P. Gumbsch, and M. Wegener, *Pentamode metamaterials with independently tailored bulk modulus and mass density.* Physical Review Applied, 2014. **2**(5): p. 054007.
17. Huang, Y., X. Lu, G. Liang, and Z. Xu, *Pentamodal property and acoustic band gaps of pentamode metamaterials with different cross-section shapes.* Physics Letters A, 2016. **380**(13): p. 1334-1338.
18. Kadic, M., T. Bückmann, N. Stenger, M. Thiel, and M. Wegener, *On the practicability of pentamode mechanical metamaterials.* Applied Physics Letters, 2012. **100**(19): p. 191901.
19. Milton, G.W. and A.V. Cherkaev, *Which elasticity tensors are realizable?* Journal of engineering materials and technology, 1995. **117**(4): p. 483-493.
20. Wu, S., Z. Luo, Z. Li, S. Liu, and L.-C. Zhang, *Topological design of pentamode metamaterials with additive manufacturing.* Computer Methods in Applied Mechanics and Engineering, 2021. **377**: p. 113708.
21. Milton, G.W. and M. Camar-Eddine, *Near optimal pentamodes as a tool for guiding stress while minimizing compliance in 3d-printed materials: A complete solution to the weak g-closure problem for 3d-printed materials.* Journal of the Mechanics and Physics of Solids, 2018. **114**: p. 194-208.
22. Jiang, S., D. Guo, L. Zhang, K. Li, B. Song, and Y. Huang, *Electropolishing-enhanced, high-precision 3D printing of metallic pentamode metamaterials.* Materials & Design, 2022. **223**: p. 111211.
23. Zhang, L., B. Song, R. Liu, et al., *Effects of structural parameters on the Poisson's ratio and compressive modulus of 2D pentamode structures fabricated by selective laser melting.* Engineering, 2020. **6**(1): p. 56-67.
24. Hedayati, R., A. Leeflang, and A. Zadpoor, *Additively manufactured metallic pentamode meta-materials.* Applied Physics Letters, 2017. **110**(9): p. 091905.

25. Zhang, L., B. Song, A. Zhao, R. Liu, L. Yang, and Y. Shi, *Study on mechanical properties of honeycomb pentamode structures fabricated by laser additive manufacturing: Numerical simulation and experimental verification.* Composite Structures, 2019. **226**: p. 111199.
26. Fan, J., L. Zhang, S. Wei, Z. Zhang, S.-K. Choi, B. Song, and Y. Shi, *A review of additive manufacturing of metamaterials and developing trends.* Materials Today, 2021.
27. Huang, Y., X. Zhang, M. Kadic, and G. Liang, *Stiffer, stronger and centrosymmetrical class of pentamodal mechanical metamaterials.* Materials, 2019. **12**(21): p. 3470.
28. Hedayati, R., N. Ghavidelnia, M. Sadighi, and M. Bodaghi, *Improving the accuracy of analytical relationships for mechanical properties of permeable metamaterials.* Applied Sciences, 2021. **11**(3): p. 1332.
29. Ghavidelnia, N., S. Jedari Salami, and R. Hedayati, *Analytical relationships for yield stress of five mechanical meta-biomaterials.* Mechanics Based Design of Structures and Machines, 2020: p. 1-23.
30. Hedayati, R., S.J. Salami, Y. Li, M. Sadighi, and A. Zadpoor, *Semianalytical geometry-property relationships for some generalized classes of pentamodelike additively manufactured mechanical metamaterials.* Physical Review Applied, 2019. **11**(3): p. 034057.
31. Amendola, A., G. Carpentieri, L. Feo, and F. Fraternali, *Bending dominated response of layered mechanical metamaterials alternating pentamode lattices and confinement plates.* Composite Structures, 2016. **157**: p. 71-77.
32. Krushynska, A., P. Galich, F. Bosia, N. Pugno, and S. Rudykh, *Hybrid metamaterials combining pentamode lattices and phononic plates.* Applied Physics Letters, 2018. **113**(20): p. 201901.
33. Cai, C., R. Guo, X. Wang, F. Sun, Z. Wang, and Z. Xu, *Effect of anisotropy on phononic band structure and figure of merit of pentamode metamaterials.* Journal of Applied Physics, 2020. **127**(12): p. 124903.
34. Kadic, M., T. Bückmann, R. Schittny, and M. Wegener, *On anisotropic versions of three-dimensional pentamode metamaterials.* New Journal of Physics, 2013. **15**(2): p. 023029.